IET Nanobiotechnology

*Research Article*

IET Journals
The Institution of Engineering and Technology

# Redox/pH dual stimuli-responsive ZnO QDs-gated mesoporous silica nanoparticles as carriers in cancer therapy

ISSN 1751-8741
Received on 21st January 2019
Revised 20th April 2019
Accepted on 7th May 2019
E-First on 3rd July 2019
doi: 10.1049/iet-nbt.2019.0031
www.ietdl.org

*Wanxia Wang[1,2,3,4], Youyun Wang[1,2,3,4], Yu Wang[1,2,3,4], Huameng Gong[1,2,3,4], Hongda Zhu[1,2,3,4], Mingxing Liu[1,2,3,4]* ✉

[1]*Key Laboratory of Fermentation Engineering (Ministry of Education), Hubei University of Technology, Wuhan 430068, People's Republic of China*
[2]*Hubei Provincial Cooperative Innovation Center of Industrial Fermentation, Hubei University of Technology, Wuhan 430068, People's Republic of China*
[3]*National '111' Center for Cellular Regulation and Molecular Pharmaceutics, Hubei University of Technology, Wuhan 430068, People's Republic of China*
[4]*Hubei Key Laboratory of Industrial Microbiology, Hubei University of Technology, Wuhan 430068, People's Republic of China*
✉ *E-mail: lmxing@hbut.edu.cn*

**Abstract:** New drug delivery system (ZnO@CMS) of the redox and pH dual-stimuli responsive based on colloidal mesoporous silica nanoparticles (CMS) has been designed, in which zinc oxide quantum dots (ZnO QDs) as a capping agent was conjugated on the surface of nanoparticles by amide bonds. The release behaviour of doxorubicin (DOX) as the model drug from ZnO@CMS (ZnO@CMS-DOX) indicated the redox and pH dual-stimuli responsive properties due to the acidic dissolution of ZnO QDs and cleavage of the disulphide bonds. The haemolysis and bovine serum albumin adsorption assays showed that the modification of ZnO QDs on the mesoporous silica nanoparticles modified by mercapto groups (CMS-SH)(ZnO@CMS) had better biocompatibility compared to CMS-SH. The cell viability and cellular uptake tests revealed that the ZnO@CMS might achieve the antitumour effect on cancer cells due to the cytotoxicity of ZnO QDs. Therefore, ZnO@CMS might be potential nanocarriers of the drug delivery system in cancer therapy. The in vivo evaluation of ZnO@CMS would be carried out in future work.

## 1 Introduction

Although the treatment of cancer has improved in the past few decades [1], current therapies mainly rely on traditional cytotoxic drugs with undesirable side effects and limited efficacy due to the similarities between cancer cells and healthy cells [2–5]. To address this formidable challenge, the diverse classes of nanoscale drug delivery systems (DDSs) have been developed in recent years, including liposomes, polymeric micelles, gold nanoparticles, carbon nanotubes, polymeric nanoparticles, quantum dots, and mesoporous silica nanoparticles (MSNs) [6–10]. Compared with the various nanoparticles, MSNs exhibit the attractive properties, such as the ease of surface functionalisation, high specific surface area, tunable pore size, high stability, and good biocompatibility [11–15]. Therefore, MSNs as the ideal candidates for the development of stimuli-responsive DDSs have been paid close attention.

The ideal stimuli-responsive DDSs should consist of the following advantages: biocompatible, high drug-loading capacity, a specific transport mechanism to protect normal cells and tissues, zero premature drug release and accurate release in response to extrinsic or intrinsic stimuli including pH, redox potential, temperature, enzyme, light, magnetic field, and ultrasound [16–22]. The disulphide bond as a redox-responsive bond can be cleaved under a high concentration of glutathione (GSH) with its advantages on the relative stability in extracellular fluids and plasma, and the easy rupture in intracellular fluid, since the concentration of GSH in tumour cells (1–10 mM) is nearly 103-fold higher than that of GSH in the plasma environment (2–20 μM) [23]. So drug can be released from the nanomaterials functionalised with a nanovalve containing a disulphide bond in specific times in tumour cells.

The zinc oxide quantum dots (ZnO QDs) are stable under neutral and physiological conditions, which can be dissociated into $Zn^{2+}$ in the acidic environment below a pH value of 6 [24–27]. Therefore, it can be used as a pH stimulus response for antitumour drugs in the mild acid environment with the extracellular environment in solid tumours (pH 6) and within the cell such as endosomes and lysosomes (pH 6.5–4.5). In addition, the ZnO QDs consist of the following advantages: firstly, they possess good fluorescent properties compared to organic dyes including narrow emission peaks, broad absorption spectra, longer-fluorescence lifetime, photobleaching resistance, tunable luminescent colours by controlling the size of particles, a wide range of solvent types and surface modification, which can be used for long-term fluorescence tracking [28–32]. Secondly, the ZnO QDs are relatively biocompatible and environmental safety compared with the cadmium-based QDs [33]. Finally, ZnO QDs have been found to have the potential for bioimaging applications related to drug delivery [34, 35]. The acid sensitive ZnO QDs as a capping agent of mesoporous silica was designed to ensure the minimum release of the drug before reaching the target site and achieve the tumour therapy.

In this work, a novel redox and pH dual stimuli responsive delivery system based on colloid MSNs (CMS) has been successfully constructed for on-demand drug release and synthesized by the following steps (shown in Fig. 1). The CMS modified by mercapto groups (CMS-SH) was synthesized by a co-condensation method with Tetraethoxysilane (TEOS) and 3-mercaptopropyl-trimethoxysilane (MPTES). The disulphide bond and carboxyl-bifunctionalised CMS (CMS-SS-COOH) was obtained by amidation reaction with maleic anhydride in the terminal of CMS-SS-$NH_2$, which was prepared with CMS-SH and *S*-(2-aminoethylthio)-2-thiopyridine hydrochloride (Py-SS-$NH_2$). Meanwhile, the $NH_2$-functionalised zinc oxide quantum dots ($NH_2$-ZnO QDs) with the water-stable, monodisperse and highly luminescent was fabricated by a novel ligand exchange-free strategy with ZnO QDs and 3-aminopropyltriethoxysilane


© The Institution of Engineering and Technology 2019

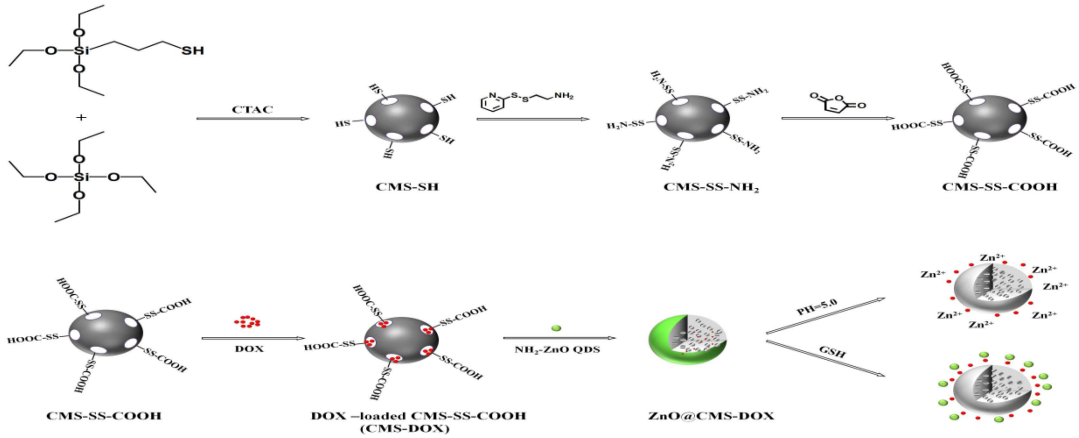


**Fig. 1** *Preparation of ZnO@CMS-DOX and drug release*

(APTES). Finally, the ZnO@CMS was prepared by amidation reaction with $NH_2$-ZnO QDs as a pH-responsive gatekeeper conjugated to the surface of CMS-SS-COOH. The doxorubicin (DOX) as the model drug from ZnO@CMS was released by the disulphide bond cleaved in GSH and rapid dissolution of ZnO QDs in the acid environment. The results of bovine serum albumin (BSA) adsorption and haemolysis assay of ZnO@CMS revealed that ZnO QDs modified on the surface of CMS-SS-COOH could improve the biocompatibility of CMS-SH by reducing the denaturation of membrane proteins with silicate, and the affinity between CMS and the tetra-alkyl ammonium groups that in red blood cell (RBC) membranes. The cellular uptake performance of ZnO@CMS-DOX showed a higher cellular uptake performance than that of DOX-loaded CMS-SS-COOH (CMS-DOX) due to the ZnO QDs as a capping agent blocking the pores of nanoparticles and inhibiting the release of DOX. These results show that nanomaterials of ZnO@CMS could be used as an attractive and promising intracellular redox/pH dual stimuli-responsive drug delivery system for therapeutic applications.

## 2 Materials and methods

### *2.1 Materials*

TEOS, BSA, GSH (98%), MPTES (98%), cysteamine hydrochloride, hexadecyltrimethylammonium chloride (CTAC), APTES, 1-ethyl-3-(3-dimethylaminopropyl)carbodiimide–hydrochloride (EDC·HCl), and 3-[4,5-dimethylthialzol-2-yl]-2,5-diphenyltetrazolium bromide (MTT) were purchased from Aladdin (China). Sodium hydroxide (NaOH), zinc acetate, magnesium acetate, *N*,*N*-dimethylformamide (DMF), absolute ethanol, methanol, acetic acid, diethyl ether, maleic anhydride, triethylamine (TEA), hexane, doxorubicin (DOX), paraformaldehyde, fluorescein diacetate (FDA), 4′,6-diamidino-2-phenylindole (DAPI), Coomassie Brilliant Blue, Rabbit red blood cells (RBCs), RPMI 1640 culture medium [Dulbecco modified eagle's medium (DMEM)], foetal bovine serum (FBS) and penicillin–streptomycin were obtained from Sinopharm Chemical Reagent Co. (China). All other chemicals were of analytical grade as required and used without further purification.

### *2.2 Preparation of CMS-SH*

The CMS-SH was synthesised using a base-catalysed sol–gel method according to the published literature [36]. The mixture of 64 ml of distilled water, 10.5 ml of absolute ethanol and 10.4 ml of 25wt% CTAC was vigorously stirred for 10 min at room temperature. Subsequently, 4.125 ml of TEA was added and the solution was stirred for 15 min. Then 40 ml of the obtained mixture solution was heated to 60 °C, followed by the drop wise addition of the mixture of 2.9 ml of TEOS and 0.32 ml of MPTES under stirring. After the solution was stirred for 2 h, the obtained colloidal suspension was centrifuged and washed twice with ethanol. The products were refluxed twice in a solution of 15 ml of HCl (37%) and 135 ml of absolute ethanol for 2 h at 60°C, and then the surfactant-removed samples were centrifuged, washed alternately with water and ethanol for 5–6 times. Finally, the resulting products were redispersed in ethanol for storage.

### *2.3 Synthesis of Py-SS-$NH_2$*

The synthesis of the compound was according to a previous report [37]. Then 4.4 g of 2,2'-dipyridyldisulphide was dissolved in 20 ml of methanol and then 0.8 ml of acetic acid was added, followed by the drop wise addition of 10 ml of methanol solution containing cysteamine hydrochloride (1.14 g) within 15 min. The mixture was stirred for an additional 48 h at room temperature and then evaporated under high vacuum to obtain a yellow oil product washed with 50 ml of diethyl ether and then dissolved in10 ml of methanol with the purification step repeated for two times with drying under vacuum for 12 h.

### *2.4 Synthesis of CMS-SS-$NH_2$*

CMS functionalised with an amino group containing the disulphide bond (CMS–SS–$NH_2$) was obtained by the following the steps: suspending 200 mg of CMS-SH in ethanol (20 ml), and then followed by the addition of 200 mg of Py-SS-$NH_2$. The mixture was stirred at room temperature for 24 h. Then the product was collected by centrifugation and washed with ethanol for three times. The resulting products were redispersed in ethanol for storage.

### *2.5 Synthesis of CMS-SS-COOH*

CMS-SS-$NH_2$ (100 mg) was dispersed in DMF solution (15 mL) and then TEA was subsequently added under stirring until the pH of the solution reached 10, followed by the drop wise addition of 2 ml of DMF solution containing 300 mg of maleic anhydride. The mixture was stirred at room temperature for another 24 h. The obtained products were centrifuged with ethanol for four times and redispersed in ethanol for storage.

### *2.6 Synthesis of ZnO QDs*

ZnO QDs were synthesised by the reported method with slight modification [38]. Zinc acetate (880 mg, 4.0 mmol) and magnesium acetate (88 mg, 0.4 mmol) were dissolved in hot ethanol (60 ml) under vigorous stirring. In a separate flask, NaOH (200 mg, 5.0 mmol) was dissolved in 20 ml of ethanol at room temperature in ultrasonic bath. The solutions were then cooled down in an ice bath. The NaOH solution was then rapidly injected into the ethanol solution containing zinc acetate and magnesium acetate. The mixture was stirred 6 h for growth of ZnO QDs. Finally, ZnO QDs were precipitated by hexane as a non-solvent and repeated this step two times.


© The Institution of Engineering and Technology 2019

### 2.7 Synthesis of $NH_2$-ZnO QDs

The obtained ZnO QDs were dispersed in 20 ml of DMF and then 100 µl of APTES was added to the solution. The mixture was reacted under stirring at 120 °C for 20 min, and then the APTES modified ZnO QDs isolated by centrifugation and washed with DMF for three times. Finally, the modified ZnO QDs were then dispersed in 10 ml of water to obtain a transparent solution.

### 2.8 Drug loading and release

20 mg of CMS-SS-COOH was dispersed into 5 ml of phosphate buffered saline (PBS) buffer solution (pH = 7.4), then 5 ml of DOX (1 mg/ml) solution was added. The resulting suspension was stirred for another 12 h at room temperature in the dark. The DOX-loaded nanoparticles of CMS-SS-COOH (CMS-DOX) were collected, washed with PBS three times. The carboxyl groups on the surface of CMS-DOX was activated by adding 33 mg of EDC·HCl at room temperature for 30 min. Then, 20 mg of $NH_2$-ZnO QDs was added drop wise to the above solution. Finally, the mixture was further stirred at room temperature for another 12 h. The CMS-DOX capped with ZnO QDs (ZnO@CMS-DOX) was obtained and washed thoroughly with water until the supernatant became colourless. The free DOX was determined in the ultraviolet–visible (UV–Vis) spectra of the supernatant and stock solutions at 480 nm. The drug loading content and drug encapsulation efficiency were calculated by following formulas:

$$\text{Drug loading content (\%)} = \frac{\text{weight of drug in nanoparticles}}{\text{weight of nanoparticles taken}} \times 100\%,$$

(see equation below) ZnO@CMS-DOX was placed in a dialysis bag, immersed in a solution with different conditions of the release environment. The release environments: (i) different concentrations of GSH (0, 0.1, 1 and 10 mM) in pH 7.4 PBS buffer solution; (ii) different pH values of PBS buffer solution (7.4, 6.0 and 5.0); (iii) 10 mM GSH in different pH PBS buffer solution (7.4, 6.0 and 5.0) with GSH 10 mM. At predetermined time intervals, 1 ml of the sample solutions were withdrawn for analysis, and equivalent fresh corresponding buffer solutions were supplemented. The calibration curve of DOX was determined by the absorbance values of different concentrations of DOX at 480 nm. The amount of released DOX was based on a calibration curve with a series of diluted pure DOX solutions. The calibration curve fits the Lambert and Beers law well: $A = 0.0194C - 0.0194$ ($R^2 = 0.9975$), where $A$ is the absorbance and $C$ is the concentration of the sample (µg/ml).

### 2.9 Haemolysis assay

The rabbit RBCs were collected from 6 ml of rabbit whole blood by centrifugation at 1000 rpm for 10 min and washed five times with sterile normal saline solution. Then 2 ml of washed RBCs diluted with sterile normal saline solution to a concentration of 2% (v/v). Then 2 ml of the diluted RBCs solution was mixed with 2 ml of CMS-SH, ZnO@CMS dispersions at the different concentrations ranging from 20 to 1500 µg/ml, respectively, and then kept static for 4 h. The mixtures were centrifuged at 1000 rpm for 10 min, and the absorbance of the supernatant was measured on a microplate reader at 541 nm. The haemolysis of RBCs in distilled water and saline was used as the positive and negative control, respectively. The haemolysis percentage was calculated through the following equation [39]: (see equation below)

### 2.10 BSA adsorption measurements

The adsorption measurement of BSA was carried out according to the published literature [40, 41]. Then 60 mg of BSA was completely dissolved in 100 ml of deionised water. Then 5 mg of CMS-SH, ZnO@CMS were dispersed in 5 ml of PBS solution, respectively, and then 5 ml of BSA solution was added. At the same time, the control group was 5 ml of PBS and 5 ml of BSA solution, and the mixture was placed on the shaker for 4 h (150 rpm, 37°C). The mixed solutions were centrifuged, and the supernatant was collected. The concentration of residual BSA solution was determined by staining with Coomassie Brilliant Blue solution. The supernatant was collected, and then diluted with 10-fold water. Then 1 ml of the diluted supernatant and 5 ml of Coomassie Brilliant Blue solution were mixed to measure the optical density (OD) value of residual BSA at 595 nm. The amount of BSA adsorbed can be calculated using the following formula [42]:

$$Q = (C_i - C_f) \times 10 \times V/m,$$

where $C_i$ and $C_f$ are the concentration of BSA in a control group and the residual BSA after adsorption, respectively; $V$ is the total volume of the solution and $m$ is the weight of the nanoparticles added to the solution.

### 2.11 Cell viability studies

MCF-7 cells were cultured in DMEM culture medium supplemented with 10% (v/v) FBS, penicillin (1%) and streptomycin (1%) in a humidified atmosphere containing 5% $CO_2$ at 37°C. The medium was routinely changed every 2 days and the cells were separated by trypsinisation before reaching confluency. The cell biocompatibility and cytotoxicity of the carrier material were evaluated by 3-[4,5-dimethylthialzol-2-yl]-2,5-diphenyltetrazolium bromide (MTT) assay. The MCF-7 cells were then incubated with various concentrations of CMS-SS-COOH, ZnO@CMS, ZnO@CMS-DOX, $Zn^{2+}$ ($ZnCl_2$), ZnO QDs and free DOX for 48 and 72 h. The materials were diluted to five gradient concentrations (based on the concentration of the nanoparticles), respectively. MCF-7 cells were seeded into 96-well plates at a density of 5 × 104 per well in 100 µl of medium and incubated for 48 and 72 h. After incubating, the cells were cultured in the medium containing 5 mg/ml of MTT for 4 h. The formazan crystals formed by the living cells was dissolved in 150 µl of dimethyl sulphoxide per well. Finally, the absorbance was measured on a microplate reader at 490 nm. Cells without any treatment served as normal control. The live/dead staining method was used to make viable cells visualised. The MCF-7 cells were seeded in a 96-well plate at a density of 5 × 104 and incubated samples with various concentrations for 48 and 72 h, then removing the medium with PBS buffer solutions washed for three times. Each well was filled with 100 µl of staining reagent containing FDA (6 mM) and propidium iodide (4 mM) for 10 min, washed twice with PBS, then added 120 µl of PBS buffer and photographed under a fluorescence microscope. The viable cells were stained green, while dead cells were stained red.

### 2.12 Cellular uptake

The fluorescence microscope was used to observe the cellular uptake of the carrier materials. The MCF-7 cells were seeded into 24-well plates at a density of 5 × 104 per well adherent for 24 h, then the medium was removed. The MCF-7 cells were incubated with DOX, CMS-DOX, and ZnO@CMS-DOX (all samples

$$\text{Drug entrapment efficiency(\%)} = \frac{\text{weight of drug in nanoparticles}}{\text{weight of drug injected}} \times 100\%.$$

$$\text{Haemolysis percentage} = \frac{\text{OD}_{\text{sample}} - \text{OD}_{\text{negative control}}}{\text{OD}_{\text{positive control}} - \text{OD}_{\text{negative control}}} \times 100\%.$$


© The Institution of Engineering and Technology 2019

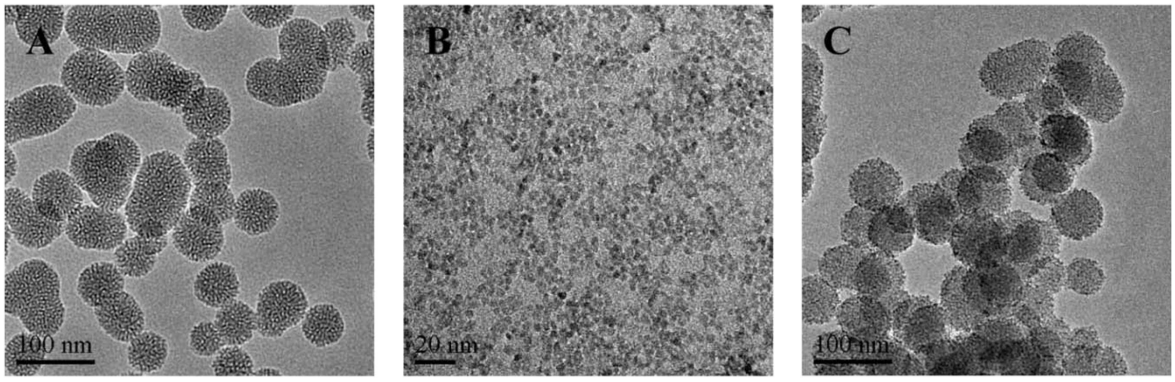


**Fig. 2** *TEM images of*
***(a)*** CMS-SS-COOH, ***(b)*** ZnO QDs, ***(c)*** ZnO@CMS

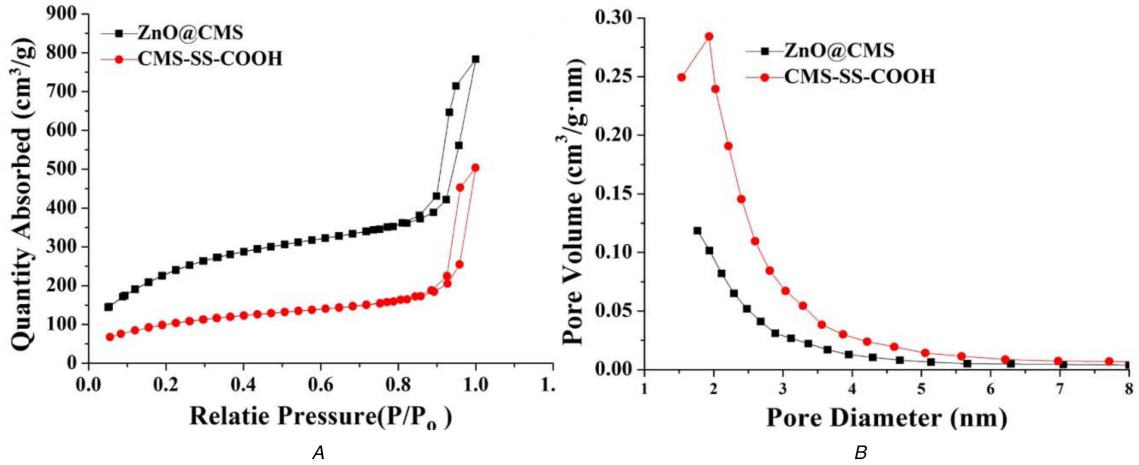


**Fig. 3** *The characterization studies of mesoporous of CMS-SS-COOH and ZnO@CMS*
***(a)*** $N_2$ adsorption–desorption isotherm, ***(b)*** Pore size distribution

containing 2 or 5 µg/ml of DOX) for 1, 2 and 4 h, respectively. The cells were washed with PBS (pH = 7.4, 0.01 mol/l) three times, and with 1 ml of 4% paraformaldehyde fixed for 15 min. After the fixative solution was removed, the cells were washed with PBS. The nuclei were stained with 1 ml of DAPI (100 ng/ml) for 10 min in the dark. Thereafter, the DAPI was removed and washed with PBS, and then the cells were placed under a fluorescence microscope to analyse the intensity of the fluorescence.

### *2.13 Characterisation*

The size and mesoporous structure of the nanoparticles were measured by transmission electron microscopy (TEM) (Tecnai G2 20 S-TWIN, FEI). The specific surface area, pore volume (VP) and pore size of each sample were obtained by nitrogen adsorption/desorption (ASAP 2020M, Mike Murray Feldman Instrument Corporation, Shanghai, China). The particle sizes and zeta potentials were measured on a Zetasizer Nano ZS90 (Malvern Instruments Ltd., Worcestershire, UK). The Fourier transform infrared (FT-IR) spectra were measured on a FT-IR spectrometer (Bruker IFS 55, Faellanden, Switzerland). The nanoparticles of crystal type were performed by X-ray diffraction (XRD; Rigaku, Japan). The fluorescence spectra were recorded on a fluorescence spectrophotometer (LS-55, Perkin Elmer, America, $\lambda_{ex} = 345$ nm). The UV–Vis absorption spectra were recorded on a Perkin Elmer Lambda 35 spectrophotometer. The fluorescence imaging was performed by using a fluorescence inverted microscope (IX73, Olympus, Japan). The absorbance of BSA adsorption, haemolysis assay, and MTT assay was recorded at 490 nm using a Biotek Epoch Flash multifunctional microplate reader.

## 3 Results and discussion

### *3.1 Preparation and characterisation of ZnO@CMS*

The synthetic process of the CMS-based nanoparticles with $NH_2$-ZnO QDs as a pH-responsive gatekeeper was displayed in Fig. 1. As shown in Fig. 2*A*, the prepared CMS-SS-COOH had a uniform spherical shape with a diameter of ∼70 nm. The TEM image showed that the CMS-SS-COOH nanoparticles were spherical in shape with a wormhole arrangement of the mesopores. As shown in Fig. 2*B*, ZnO QDs had a uniform spherical shape with an average diameter of ∼3–4 nm. The mesoporous structure of ZnO@CMS could not be clearly observed in Fig. 2*C*. The result revealed that the entrance of the mesopore on the outer surface of CMS-SS-COOH was tightly covered with $NH_2$-ZnO QDs. The $N_2$ adsorption–desorption isotherm and pore size distribution curves of CMS-SS-COOH and ZnO@CMS are shown in Fig. 3. The Brunauer–Emmett–Teller (BET) surface area, total VP, and Barrett–Joyner–Halenda pore size distribution are summarised in Table 1. As shown in Fig. 3*A*, the two kinds of nanoparticles show typical IV mesoporous. By the corresponding formula calculation, the BET specific surface area of CMS-SS-COOH and ZnO@CMS was 864 and 363 $m^2/g$, respectively. The VP was 1.21 and 0.78 $cm^3/g$, respectively. The specific surface area and VP of ZnO@CMS were significantly smaller than that of CMS-SS-COOH due to the ZnO QDs grafted onto the surface of mesoporous silica with the pores blocked. The pore size distribution of CMS-SS-COOH and ZnO@CMS is shown in Fig. 3*B*. Compared with the pore diameter of CMS-SS-COOH, the pore diameter of ZnO@CMS was decreased from 2.1 to <2 nm. These results indicated that ZnO QDs as an effective capping agent of MSNs might prevent drug leakage.

The photoluminescence (PL) spectra of the prepared samples were recorded in aqueous solution at room temperature and the excitation wavelength of 345 nm is shown in Fig. 4*A*. The ZnO QDs exhibit a yellow–green emission peak at 520 nm due to the


© The Institution of Engineering and Technology 2019

**Table 1** Nitrogen adsorption–desorption analysis of CMS-SS-COOH and ZnO@CMS

| Samples | Surface area ($m^2$/g) | VP ($cm^3$/g) | Pore size (nm) |
|---|---|---|---|
| CMS-SS-COOH | 864 | 1.21 | 2.1 |
| ZnO@CMS | 363 | 0.78 | <2 |

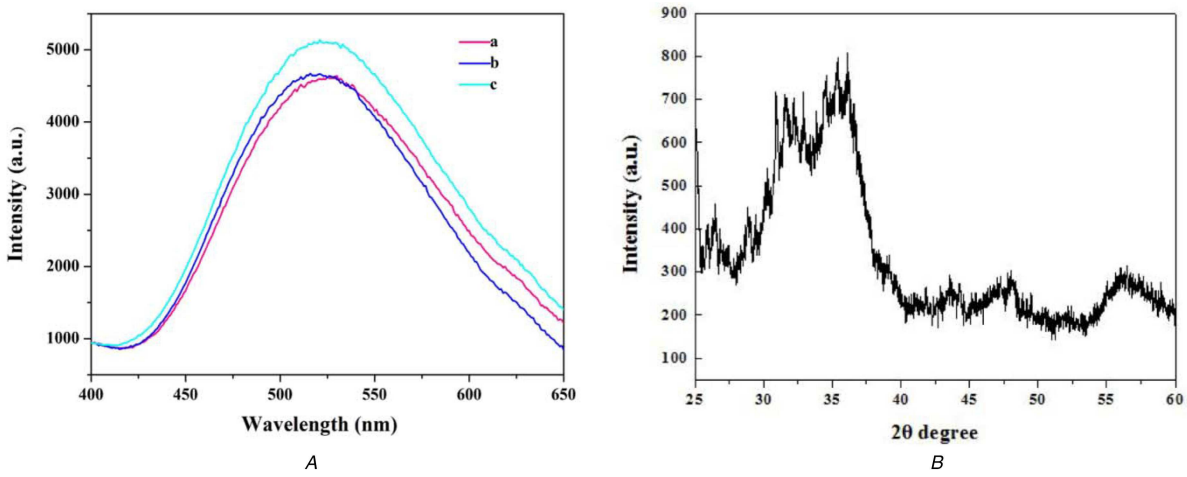


**Fig. 4** *The photoluminescence (PL) spectra and XRD pattern of*
***(a)*** PL spectra of ZnO@CMS (a), ZnO QDs (b), ZnO-$NH_2$ QDs (c), ***(b)*** The XRD pattern of ZnO QDS

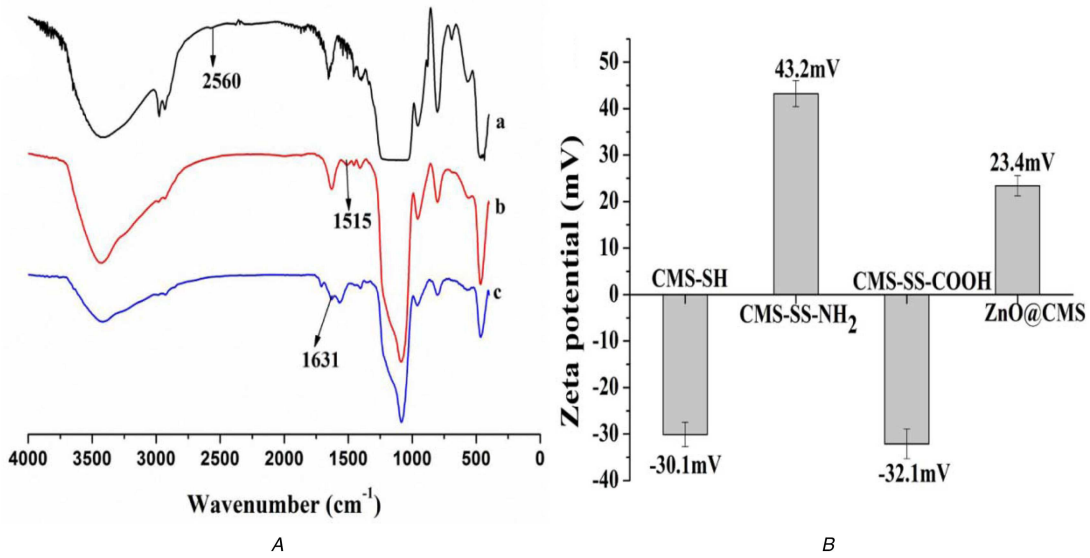


**Fig. 5** *he FT-IR spectra and zeta potential of nanoparticls*
***(a)*** The FT-IR spectra of CMS-SH (a), CMS-SS-$NH_2$ (b) and CMS-SS-COOH (c), ***(b)*** The zeta potential of CMS-SH, CMS-SS-$NH_2$, CMS-SS-COOH and ZnO@CMS

plasmon resonance on the surface. Compared to ZnO QDs, the intensity of fluorescence emission of $NH_2$-ZnO QDs was enhanced with no obvious changes of the emission wavelength due to the modification of amino groups on ZnO QDs could effectively reduce the surface defects. ZnO@CMS also showed obvious yellow–green emission contributed to the fluorescence of ZnO QDs at the same position, indicating that ZnO QDs were successfully covered on the surface of CMS-SS-COOH. The intensity of PL of ZnO@CMS was slightly decreased compared with the ZnO QDs due to the electrostatic interaction between amino groups of $NH_2$-ZnO QDs and the carboxyl group on the surface of CMS-SS-COOH. The powder wide-angle X-ray diffraction of ZnO QDs is shown in Fig. 4*B*, the typical peaks characteristic of the ZnO hexagonal wurtzite structure was displayed and in consistent with the previously reported literature [43].

The FT-IR spectra of CMS-SH, CMS-SS-$NH_2$, and CMS-SS-COOH are shown in Fig. 5*A*. CMS-SH showed a minimum peak at 2560 $cm^{-1}$ attributed to the characteristic peak of mercapto groups with the characteristic peaks of Si–O–Si and Si–OH remained. CMS-SS-$NH_2$ showed a new adsorption peak at 1515 $cm^{-1}$ while the minor peak of thiol groups around 2560 $cm^{-1}$ disappeared, indicating the formation of CMS-SS-$NH_2$. Compared with CMS-SS-$NH_2$, CMS-SS-COOH showed a sharp new peak at 1631 $cm^{-1}$ while retaining the characteristic peak of silica, which is attributed to the stretching vibration of the carbonyl group. As shown in Fig. 5*B*, owing to the amino group in CMS-SS-$NH_2$, the zeta potential value of CMS-SH reverses from a negative value of −30.1 mV to a positive value of 43.2 mV. The ζ-potential value reversed to a negative value of −32.1 mV by the introduction of the carboxyl group. The zeta potential finally reversed to 23.4 mV after $NH_2$-ZnO QDs grafted on the surface of CMS-SS-$NH_2$. The result further supported the observation of FT-IR spectra and demonstrated successful functionalisation.

### *3.2 In vitro release behaviour*

Since the large VP of CMS-SS-COOH and the high encapsulation ability of ZnO QDs gatekeeper, the highest drug loading efficiency


© The Institution of Engineering and Technology 2019

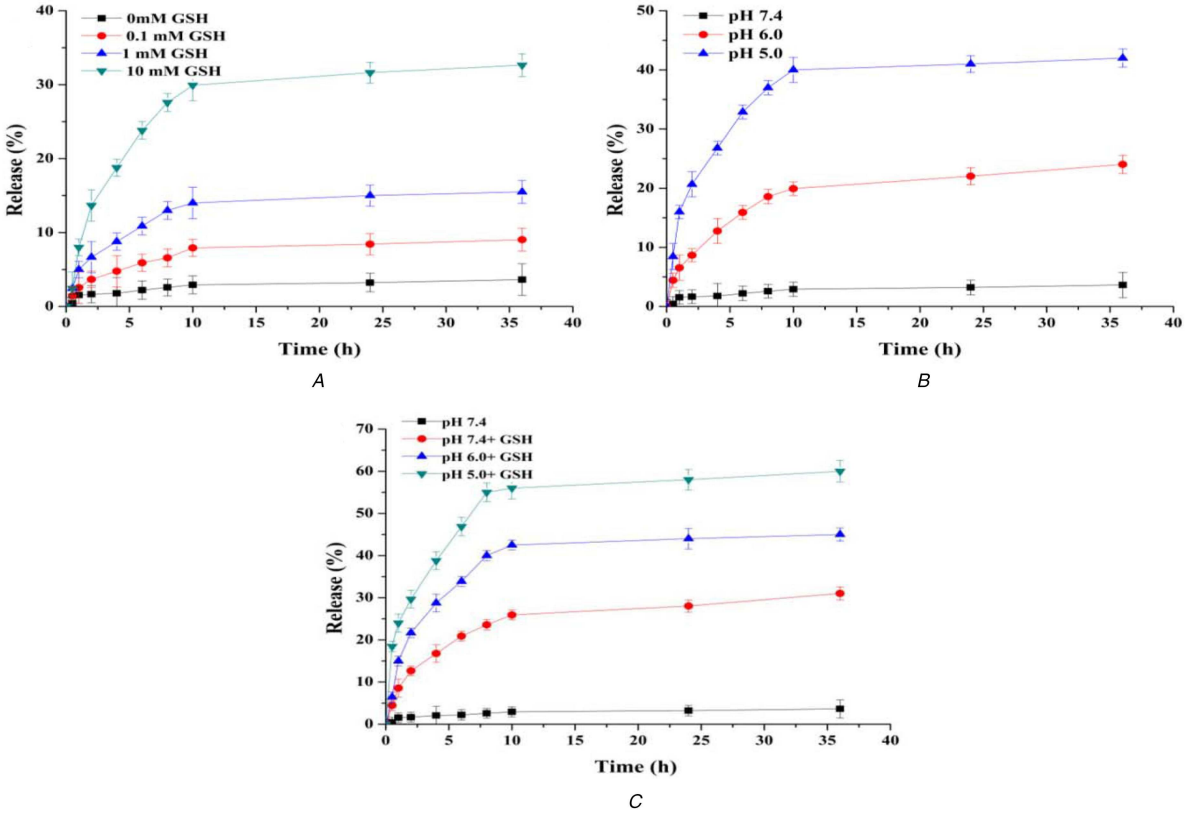


**Fig. 6** *Release of DOX from the ZnO@CMS*

***(a)*** In PBS buffer solution at pH 7.4 of different concentrations of GSH, ***(b)*** Different pH values, ***(c)*** pH and GSH triggered synergistic release profiles in PBS buffer solution at different pH with the concentration of GSH at 10 mM

and encapsulation efficiency of ZnO@CMS-DOX were up to 6.09 and 97.58%, respectively. As shown in Fig. 6*A*, ~3.63% DOX released from ZnO@CMS within 36 h at physiological pH without GSH, indicating that the ZnO QDs could completely cover the surface of mesoporous silica. The amount of DOX released significantly increased with the increasing concentration of GSH. The rate of DOX release was relatively fast within 10 h, the cumulative release of DOX reached 32.4% within 36 h. The cumulative release of DOX reached 18.7% within 4 h in 10 mM GSH due to the cleavage of disulphide bonds. Therefore, the obtained ZnO@CMS as an effective drug carrier had the ability to control the drug release by GSH. In Fig. 6*B*, the amount of DOX release was significantly increased and the release rate relatively faster within 8 h with the acidic increasing. Since the ZnO QDs were stable at pH 7.4 and dissolved rapidly at pH < 5.5, the cumulative release reached 22.03% in pH 5.0 and 42% in pH 6.0 within 36 h, respectively. The release behaviour affected by GSH and pH is shown in Fig. 6*C*, the concentration of GSH was 10 mM, the cumulative release reached up to 60% within 36 h in pH 5 and the drug release rate was promoted with the acidic increasing. Compared with Figs. 6*A* and *B*, the dual response of drug release efficiency was significantly higher than that of the single pH or redox responsive. Therefore, the grafting of ZnO QDs on the surface of CMS-SS-COOH via amide linkage could possibly render the carrier with acid-responsive and GSH responsive capability, which might be an effective drug carrier for the delivery system.

### *3.3 Haemolytic Behaviour and BSA adsorption of CMS-SH and ZnO@CMS*

A haemolysis test was considered as a simple and reliable measure to evaluate the biocompatibility of materials. It has been reported that haemolysis up to 5% was allowed for biomaterials [44]. The haemolysis images of CMS-SH and ZnO@CMS over the concentration range of 20–1500 μg/ml are shown in Fig. 7*A*. The ZnO@CMS nanoparticles showed excellent dispersibility and stability in high concentrations of normal saline up to 1500 μg/ml. The haemolysis results for CMS-SH and ZnO@CMS are shown in Fig. 7*B*. When the concentration of CMS-SH reached 1500 μg/ml, the percentage haemolysis reached 87%. The haemolysis percentage of CMS-SH was so high due to the reactive oxygen species (ROS) induced by the surface of the silica [45, 46], the electrostatic interaction between the silanol groups with the membrane protein, affinity between the silicate with the tetra-alkyl-ammonium groups present in the membrane of RBCs [47]. The high degree of haemolysis raised serious safety concerns regarding the application of nanomaterials for drug delivery. Therefore, the modification of ZnO QDs on the surface of CMS could improve the biocompatibility of CMS-SH by reducing the electrostatic interactions, and the affinity between CMS and the tetra-alkyl-ammonium groups. As expected, the haemolysis percentage of ZnO@CMS was decreased significantly to 3.6% at an extremely high concentration of 1500 μg/ml. Therefore, the ZnO QDs modified on the CMS-SH could improve the biocompatibility of nanomaterials.

It has been reported that BSA could be non-specific and adsorbed by MSNs [48]. As shown in Fig. 7*C*, the amounts of BSA adsorbed by CMS-SH and ZnO@CMS were 15.2 and 3.2 wt%, respectively. Compared with CMS-SH, the amount of BSA adsorbed on to ZnO@CMS was decreased significantly by 12%. The result indicated that ZnO QDs modified on the CMS-SH might decrease the adsorption of BSA by changing the chargeability on the surface of nanomaterials.

### *3.4 Cytotoxicity assay*

The viability of MCF-7 cells cultured with ZnO QDs and the corresponding concentration of $Zn^{2+}$ ions ($ZnCl_2$) were studied. As shown in Figs. 8*A* and *C*, the cell viability of both samples has the same trend, and the cell viability decreased below 20% by extending the time when their concentrations above 20 μg/ml. The greater cytotoxicity of ZnO QDs might be on account of the ROS production, lipid peroxidation and DNA damage by $Zn^{2+}$ by the intracellular dissolution of ZnO QDs [49]. The cytotoxicity of other samples (CMS-SS-COOH, ZnO@CMS, ZnO@CMS-DOX,


© The Institution of Engineering and Technology 2019

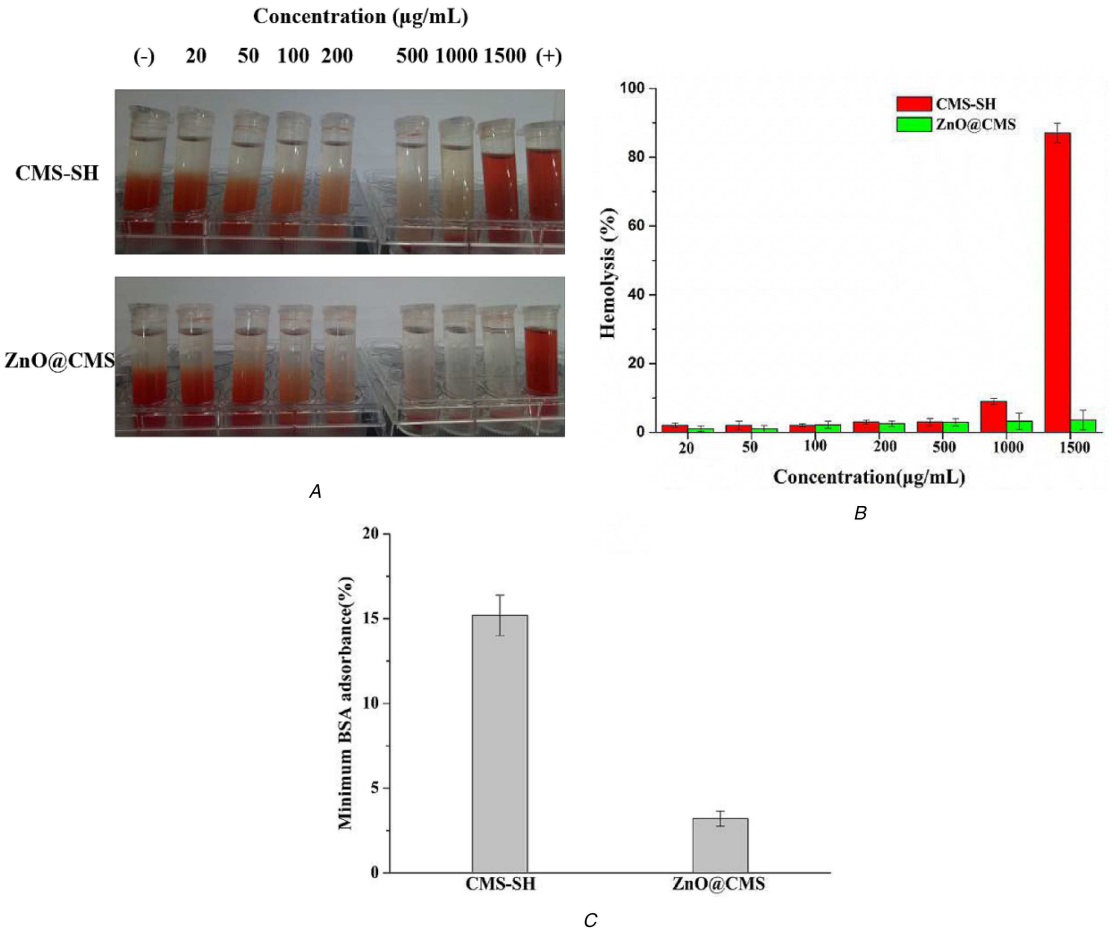


**Fig. 7** *Hemolytic behavior and BSA adsorption of CMS-SH and ZnO@CMS*
***(a)*** Haemolytic photographs, ***(b)*** Haemolysis percentages, ***(c)*** BSA absorbance

free DOX) was evaluated by MTT assay. As shown in Figs. 8*B* and *D*, the CMS-SS-COOH showed no obvious cytotoxicity at a concentration of 100 μg/ml, while the cell viability of ZnO@CMS decreased to 27% at a the same concentration by the ZnO QDs dissolved in $Zn^{2+}$ in tumour cells at 48 h. It was demonstrated that the cell viability of ZnO@CMS-DOX was <20% at a concentration of 50 μg/ml and more effective than free DOX at 48 h. The cell viability decreased with extending the time, and when their concentrations were 100 μg/ml, the cell viability of ZnO@CMS-DOX decreased below 10% at 72 h. These results revealed that the redox and pH dual stimuli-responsive could promote the rapid release of the drug and show the corresponding toxicity. Therefore, the constructed ZnO@CMS delivery system had a broad application prospect in chemotherapy specific to the tumour site. The cell viabilities were further visualised by live/dead fluorescence imaging shown in Fig. 9. Nearly all of the cells were stained green (live cells) at a different concentration of samples, a part of cells was stained red (dead cells) when treated with a high concentration of samples. The obtained results reflected by the fluorescence images were in consistent with the results of MTT assay.

### *3.5 Cellular uptake*

The intracellular uptake of DOX, CMS-DOX, and ZnO@CMS-DOX incubated with MCF-7 cells is shown in Fig. 10. With the concentration of samples increasing, the intracellular DOX fluorescence intensity was stronger in 5 μg/ml than in 2 μg/ml and the fluorescence intensity of samples in MCF-7 cells at 6 h was obviously stronger than at 2 and 4 h. The results indicated that the cellular uptake of ZnO@CMS-DOX appeared in time and concentration-dependent pattern. The CMS-DOX has a relatively weak fluorescence due to the pores of CMS-DOX without blocked by ZnO QDs and leading to the leakage of DOX. The red fluorescence of ZnO@CMS-DOX was mainly presented in the cytoplasm, and slowly diffuses into the nucleus with time and the red fluorescence of the free DOX was presented in the nucleus, indicating that DOX loaded nanomaterials diffused into the nucleus and then released intracellularly.

## 4 Conclusions

In this study, we have successfully prepared the redox/pH dual-stimuli responsive drug delivery systems based on mesoporous silica nanoparticles grafted with $NH_2$–ZnO QDs as a gatekeeper by the amidation reaction for effective control of the drug release. The in vitro release studies indicated the redox and pH-sensitive drug release behaviours. The haemolysis and BSA adsorption experiments showed that the modification of ZnO QDs on CMS-SH (ZnO@CMS) has better biocompatibility compared to CMS-SH. The cell viability assay exhibited that the ZnO@CMS might achieve an antitumour effect on cancer cells due to the cytotoxicity of ZnO QDs. The ZnO@CMS-DOX showed a higher cellular uptake performance in MCF-7 cells than that of CMS-DOX due to the ZnO QDs as a capping agent blocking the pores of nanoparticles and inhibiting the release of DOX. Therefore, the excellent properties of ZnO@CMS might make it the excellent redox/pH-responsive nanocarrier for broad application in tumour chemotherapy.

## 5 Acknowledgments

This work was supported by the National Natural Science Foundation of China (no. 81201197). We thank Prof. Xincai Xiao of the Analytic and Testing Center of South-Central University for Nationalities for the measurements of TEM and Prof. Qingzhi Wu of the Analytic and Testing Center of the Wuhan University of Technology for the measurements of XRD and nitrogen adsorption–desorption.


© The Institution of Engineering and Technology 2019

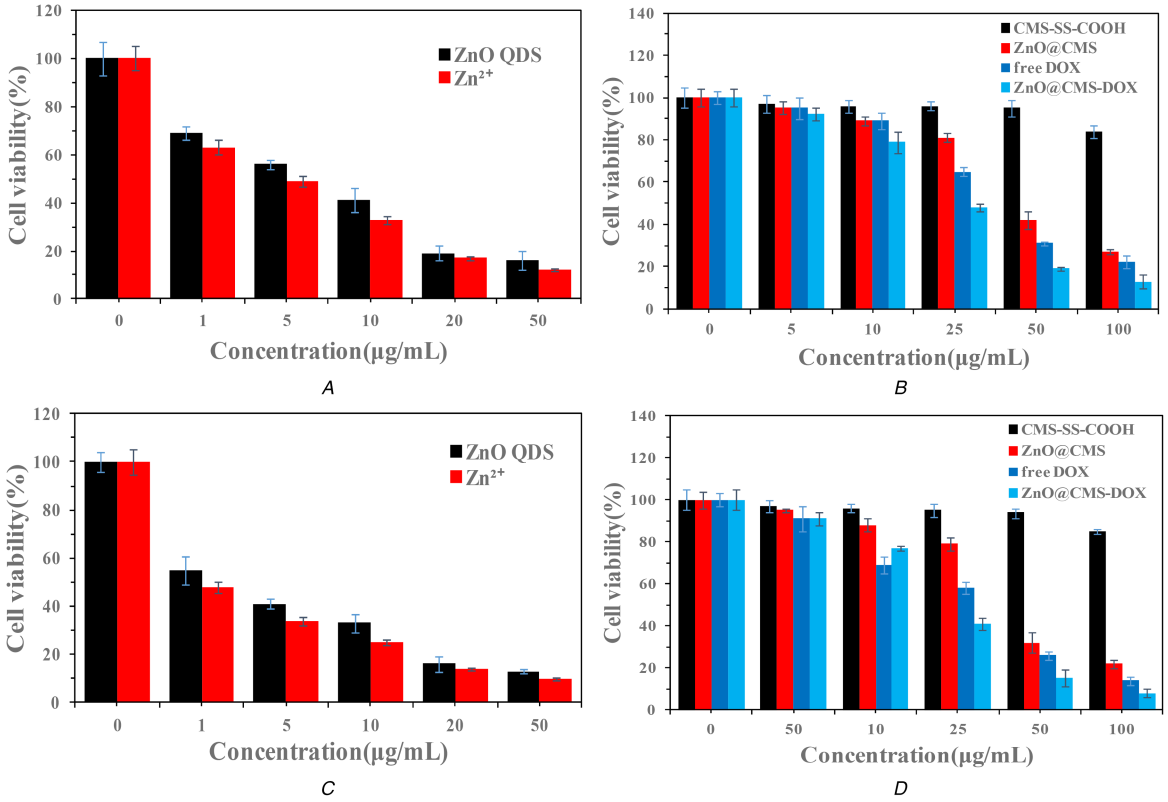


**Fig. 8** *Cytotoxicity assay*

***(a)***, ***(c)*** Viabilities of the MCF-7 cells after being incubated with ZnO QDs and $Zn^{2+}$ for 48 and 72 h, respectively, ***(b)***, ***(d)*** Viabilities of the MCF-7 cells after being incubated with CMS-SS-COOH, ZnO@CMS, ZnO@CMS-DOX and free DOX for 48 and 72 h, respectively

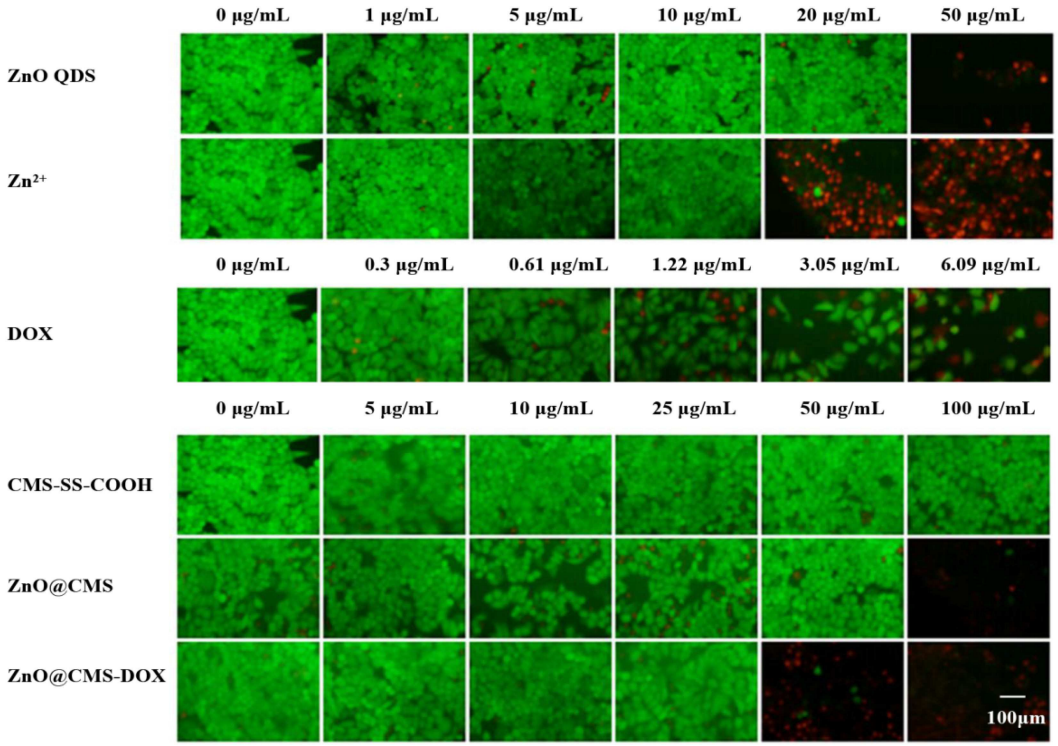


**Fig. 9** *Fluorescence images of MCF-7 cells after being incubated with $Zn^{2+}$, ZnO QDS, free DOX, ZnO@CMS, CMS-SS-COOH and ZnO@CMS-DOX with different concentrations for 24 h. The live cells were stained green, and the red indicates the dead cells*


© The Institution of Engineering and Technology 2019

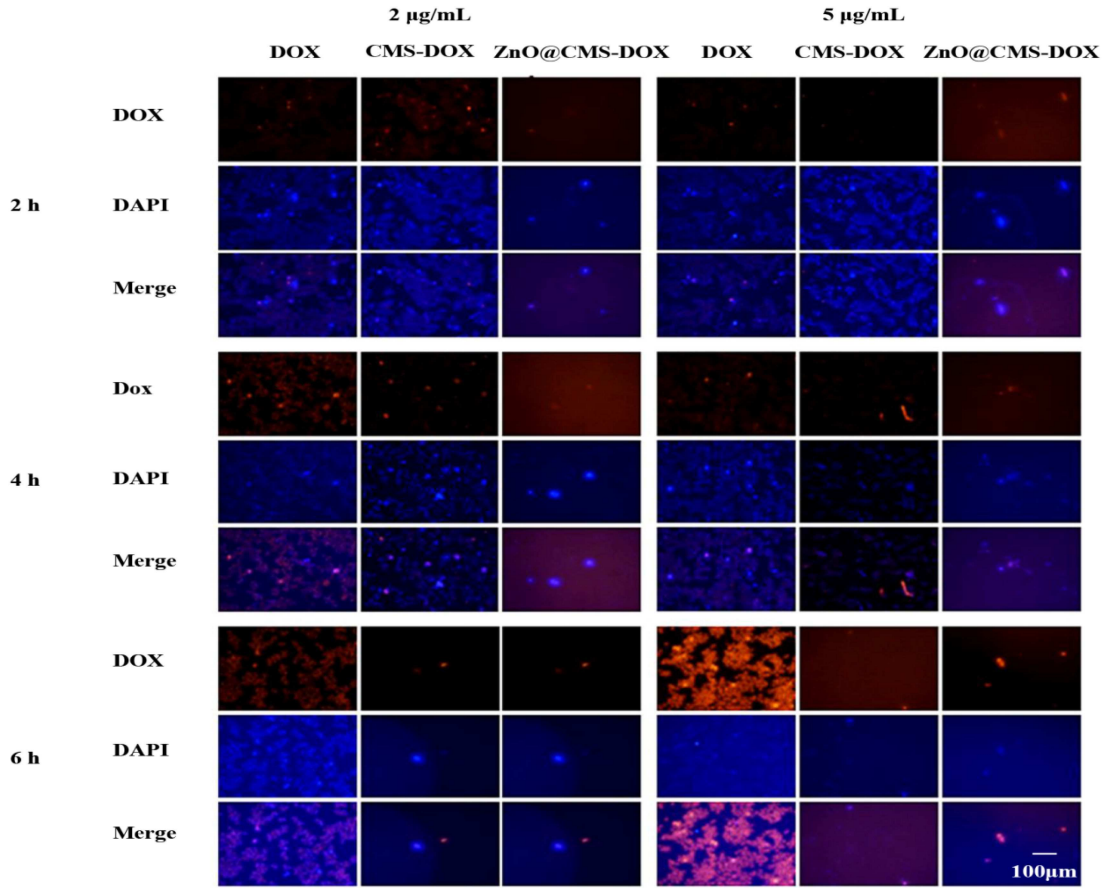


**Fig. 10** *Fluorescence microscopy images of free DOX and DOX loaded with nanoparticles with different concentrations incubated with MCF-7 cells for 2, 4 and 6 h. Nuclei were stained with blue DAPI, DOX showed red fluorescence, and the following images showed the combined fluorescence*

## 6 References


[1] Siegel, R.L., Miller, K.D., Fedewa, S.A., *et al.*: 'Colorectal cancer statistics', *CA Cancer J. Clin.*, 2017, **67**, (3), pp. 177–193

[2] Emmenegger, U., Kerbel, R.S.: 'Cancer: chemotherapy counteracted', *Nature*, 2010, **468**, (7324), pp. 637–638

[3] Karimi, M., Ghasemi, A., Sahandi, Z.P., *et al.*: 'Smart micro/nanoparticles in stimulus-responsive drug/gene delivery systems', *Chem. Soc. Rev.*, 2016, **45**, (5), pp. 457–1501

[4] Abouelkacem, L., Wilson, K.E., Johnson, S.M., *et al.*: 'Ultrasound molecular imaging of the breast cancer neovasculature using engineered fibronectin scaffold ligands: A novel class of targeted contrast ultrasound agent', *Theranostics*, 2016, **6**, (11), pp. 1740–1752

[5] Fan, C.H., Cheng, Y.H., Ting, C.Y., *et al.*: 'Ultrasound/magnetic targeting with SPIO-DOX-microbubble complex for image-guided drug delivery in brain tumors', *Theranostics*, 2016, **6**, (10), pp. 1542–1556

[6] Susewind, M., Schilmann, A.M., Heim, J., *et al.*: 'Silica-coated Au@ZnO Janus particles and their stability in epithelial cells', *J. Mater. Chem. B*, 2015, **3**, (9), pp. 1813–1822

[7] Wang Y, X., Hussain S, M., Krestin, G.P., *et al.*: 'Superparamagnetic iron oxide contrast agents: physicochemical characteristics and applications in MR imaging', *Eur. Radiol.*, 2001, **11**, (11), pp. 2319–2331

[8] Bianco, A., Kostarelos, K., Prato, M., *et al.*: 'Applications of carbon nanotubes in drug delivery', *Curr. Opin. Chem. Biol.*, 2005, **9**, (6), pp. 674–679

[9] Bruchez, M.Jr., Moronne, M., Gin, P., *et al.*: 'Semiconductor nanocrystals as fluorescent biological labels', *Science*, 1998, **281**, (5385), pp. 2013–2016

[10] Lu, J., Liong, M., Zink, J.I., *et al.*: 'Mesoporous silica nanoparticles as a delivery system for hydrophobic anticancer drugs', *Small*, 2007, **3**, (8), pp. 1341–1346

[11] Vallet-Regi, M., Rámila, A., Real, R.P.D., *et al.*: 'A new property of MCM-41: drug delivery system', *Chem. Mater.*, 2001, **13**, (2), pp. 308–311

[12] Félix, S., Lluís, P., Mar, O., *et al.*: 'Gated silica mesoporous materials in sensing applications', *Chemistryopen*, 2015, **4**, (4), pp. 418–437

[13] Zhao, W., Gu, J., Zhang, L., *et al.*: 'Fabrication of uniform magnetic nanocomposite spheres with a magnetic core/mesoporous silica shell structure', *J. Am. Chem. Soc.*, 2005, **127**, (25), pp. 8916–8917

[14] Wei, J., Wang, H., Deng, Y., *et al.*: 'Solvent evaporation induced aggregating assembly approach to three-dimensional ordered mesoporous silica with ultralarge accessible mesopores', *J. Am. Chem. Soc.*, 2011, **133**, (50), pp. 20369–20377

[15] Liu, R., Zhang, Y., Zhao, X., *et al.*: 'pH-Responsive nanogated ensemble based on gold-capped mesoporous silica through an acid-labile acetal linker', *J. Am. Chem. Soc.*, 2010, **132**, (5), pp. 1500–1501

[16] Liu, J., Detrembleur, C., Mornet, S., *et al.*: 'Design of hybrid nanovehicles for remotely triggered drug release: an overview', *J. Mater. Chem. B*, 2015, **3**, (30), pp. 6117–6147

[17] Khandare, J., Calderon, M., Dagia, N.M., *et al.*: 'Cheminform abstract: multifunctional dendritic polymers in nanomedicine: opportunities and challenges', *Chem. Soc. Rev.*, 2012, **43**, (27), pp. 2824–2848

[18] Wu, H.Q., Wang, C.C.: 'Biodegradable smart nanogels: a new platform for targeting drug delivery and biomedical diagnostics', *Langmuir ACS J. Surf. Colloids*, 2016, **32**, (25), pp. 6211–6225

[19] Kamaly, N., Yameen, B., Wu, J., *et al.*: 'Degradable controlled-release polymers and polymeric nanoparticles: mechanisms of controlling drug release', *Chem. Rev.*, 2016, **116**, (4), pp. 2602–2663

[20] Karimi, M., Zangabad, P.S., Ghasemi, A., *et al.*: 'Temperature-responsive smart nanocarriers for delivery of therapeutic agents: applications and recent advances', *ACS Appl. Mater. Interfaces*, 2016, **8**, (33), pp. 21107–21133

[21] Gulzar, A., Gai, S., Yang, P., *et al.*: 'Stimuli responsive drug delivery application of polymer and silica in biomedicine', *J. Mater. Chem. B*, 2015, **3**, (44), pp. 8599–8622

[22] Chang, Y., Yang, K., Wei, P., *et al.*: 'Cationic vesicles based on amphiphilic pillararene capped with ferrocenium: a redox-responsive system for drug/siRNA co-delivery', *Angew. Chem.*, 2014, **53**, (48), pp. 13126–13130

[23] Mezghrani, O., Tang, Y., Ke, X., *et al.*: 'Hepatocellular carcinoma dually-targeted nanoparticles for reduction triggered intracellular delivery of doxorubicin', *Int. J. Pharm.*, 2015, **478**, (2), pp. 553–568

[24] Yuan, Q., Hein, S., Misra, R.D.K., *et al.*: 'New generation of chitosan-encapsulated ZnO quantum dots loaded with drug: synthesis, characterization and in vitro drug delivery response', *Acta Biomater.*, 2010, **6**, (7), pp. 2732–2739

[25] Yuan, Q., Shah, J., Hein, S., *et al.*: 'Controlled and extended drug release behavior of chitosan-based nanoparticle carrier', *Acta Biomater.*, 2010, **6**, (3), pp. 1140–1148

[26] Zhang, P., Liu, W.: 'ZnO QD@PMAA-co-PDMAEMA nonviral vector for plasmid DNA delivery and bioimaging', *Biomaterials*, 2010, **31**, (11), pp. 3087–3094

[27] Barick, K.C., Nigam, S., Bahadur, D., *et al.*: 'Nanoscale assembly of mesoporous ZnO: A potential drug carrier', *J. Mater. Chem.*, 2010, **20**, (31), pp. 6446–6452

[28] Nguyen, D., Jiang, S., He, C., *et al.*: 'Elevating biomedical performance of ZnO/SiO2@amorphous calcium phosphate – bioinspiration making possible the impossible', *Adv. Funct. Mater.*, 2016, **26**, (38), pp. 6921–6929

[29] Tang, X., Choo, E.S.G., Li, L., *et al.*: 'Synthesis of ZnO nanoparticles with tunable emission colors and their cell labeling applications', *Chem. Mater.*, 2010, **22**, (11), pp. 3383–3388

[30] Hu, Z., Oskam, G., Searson, P.C., *et al.*: 'Influence of solvent on the growth of ZnO nanoparticles', *J. Coll. Interface Sci.*, 2003, **263**, (2), pp. 454–460




© The Institution of Engineering and Technology 2019

[31] Moussodia, R.O., Balan, L., Merlin, C., *et al.*: 'Biocompatible and stable ZnO quantum dots generated by functionalization with siloxane-core PAMAM dendrons', *J. Mater. Chem.*, 2010, **20**, (6), pp. 1147–1155
[32] Xiong, H.M., Xu, Y., Ren, Q.G., *et al.*: 'Stable aqueous ZnO@polymer core-shell nanoparticles with tunable photoluminescence and their application in cell imaging', *J. Am. Chem. Soc.*, 2008, **130**, (24), pp. 7522–7523
[33] Bagalkot, V., Zhang, L., Levy-Nissenbaum, E., *et al.*: 'Quantum dot-aptamer conjugates for synchronous cancer imaging, therapy, and sensing of drug delivery based on bi-fluorescence resonance energy transfer', *Nano Lett.*, 2007, **7**, (10), pp. 3065–3070
[34] Sato, M., Harada, H., Morito, S., *et al.*: 'Preparation, characterization and properties of novel covalently surface-functionalized zinc oxide nanoparticles', *Appl. Surf. Sci.*, 2010, **256**, (14), pp. 4497–4501
[35] Xiong, H.M.: 'ZnO nanoparticles applied to bioimaging and drug delivery', *Cheminform*, 2013, **44**, (49), pp. 5329–5335
[36] Kobler, J., Moller, K., Bein, T.: 'Colloidal suspensions of mercapto-functionalized nanosized mesoporous silica', *J. Mater. Chem.*, 2007, **17**, (7), pp. 624–631
[37] Ebright, Y.W., Chen, Y., Younggyu Kim, A., *et al.*: 'S-[2-(4-azidosalicylamido) ethylthio]-2-thiopyridine: radioiodinatable, cleavable, photoactivatible cross-linking agent', *Bioconjugate Chem.*, 1996, **7**, (3), pp. 380–384
[38] Muhammad, F., Guo, M., Qi, W., *et al.*: 'pH-Triggered controlled drug release from mesoporous silica nanoparticles via intracellular dissolution of ZnO nanolids', *J. Am. Chem. Soc.*, 2011, **133**, (23), pp. 8778–8781
[39] Zhao, L.H., Zhang, J., Sun, S.Q., *et al.*: 'Stable aqueous ZnO nanoparticles with green photoluminescence and biocompatibility', *J. Lumin.*, 2012, **132**, (10), pp. 2595–2598
[40] He, Q., Zhang, J., Shi, J., *et al.*: 'The effect of PEGylation of mesoporous silica nanoparticles on nonspecific binding of serum proteins and cellular responses', *Biomaterials*, 2010, **31**, (6), pp. 1085–1092
[41] Gu, J., Su, S., Zhu, M., *et al.*: 'Targeted doxorubicin delivery to liver cancer cells by PEGylated mesoporous silica nanoparticles with a pH-dependent release profile', *Microporous Mesoporous Mater.*, 2012, **161**, (5), pp. 160–167
[42] Zhao, Q., Geng, H., Wang, Y., *et al.*: 'Hyaluronic acid oligosaccharide modified redox-responsive mesoporous silica nanoparticles for targeted drug delivery', *ACS Appl. Mater. Interfaces*, 2014, **6**, (22), pp. 20290–20299
[43] Manaia, E.B., Caetano, B.L., Briois, V., *et al.*: 'Surface modified Mg-doped ZnO QDs for biological imaging', *Eur. J. Nanomed.*, 2015, **7**, (2), pp. 109–120
[44] Kronenthal, R.L., Oser, Z., Martin, E., *et al.*: '*Polymers in medicine and surgery*' (Plenum Press, Boston, USA, 1975), pp. 119–137
[45] Nash, T., Allison, A.C., Harington, J.S., *et al.*: 'Physico-chemical properties of silica in relation to its toxicity', *Nature*, 1966, **210**, (210), pp. 259–261
[46] Slowing, I.I., Wu, C.W., Vivero-Escoto, J.L., *et al.*: 'Mesoporous silica nanoparticles for reducing hemolytic activity towards mammalian red blood cells', *Small*, 2009, **5**, (1), pp. 57–62
[47] Depasse, J., Warlus, J.: 'Relation between the toxicity of silica and its affinity for tetraalkylammonium groups. Comparison between $SiO_2$, and $TiO_2$', *J. Coll. Interface Sci.*, 1976, **56**, (3), pp. 618–621
[48] Claesson, P.M., Blomberg, E., Fröberg, J.C., *et al.*: 'Protein interactions at solid surfaces', *Adv. Colloid Interface Sci.*, 1995, **57**, pp.161–227
[49] Deng, X., Luan, Q., Chen, W., *et al.*: 'Nanosized zinc oxide particles induce neural stem cell apoptosis', *Nanotechnology*, 2009, **20**, (11), pp. 115101–115107


© The Institution of Engineering and Technology 2019